Materials Today Chemistry 33 (2023) 101715

Contents lists available at ScienceDirect

Materials Today Chemistry

journal homepage: www.journals.elsevier.com/materials-today-chemistry/

HEMA-based macro and microporous materials for CO_2 capture

Chiara Zagni [a,**], Alessandro Coco [a], Sandro Dattilo [b,***], Vincenzo Patamia [a], Giuseppe Floresta [a], Roberto Fiorenza [c], Giusy Curcuruto [b], Tommaso Mecca [d], Antonio Rescifina [a,*]

[a] Department of Drug and Health Sciences, University of Catania, V.le A. Doria 6, 95125, Catania, Italy
[b] Institute for Polymers, Composites, and Biomaterials CNR-IPCB, Via Paolo Gaifami 18, 95126, Catania, Italy
[c] Department of Chemical Sciences, University of Catania, V.le A. Doria 6, 95125, Catania, Italy
[d] Institute of Biomolecular Chemistry CNR-ICB, Via Paolo Gaifami 18, 95126, Catania, Italy

ARTICLE INFO

Keywords:
CO_2
HEMA
Cryogel
Hydrogel
Polymer
Gas adsorption
Synthesis

ABSTRACT

New polymeric macroporous materials based on poly 2-hydroxyethyl methacrylate (pHEMA) were synthesized and tested to adsorb CO_2. To this purpose, bio and affordable amine-based molecules such as lysine (LYS) and histidine (HIS) were selected as CO_2 active sites and used to functionalize HEMA monomer before its crosslinking polymerization. The as-prepared monomers and polymers were characterized by using Nuclear Magnetic Resonance (NMR), Fourier Infrared Spectroscopy (FT-IR), Thermal gravimetric analysis (TGA), and Scanning Electron Microscopy (SEM) equipped with Energy Dispersive X-ray (EDX). Compared to materials reported in the recent literature, all produced ones provide exceptional adsorption capacity in the 162–193 ppm range. In particular, H-HEMA-LYS exhibits the best adsorption grade, well-fitting the Linear Driving Force (LFD) model. H-HEMA-LYS reusability was also tested for up to 5 cycles without significant loss in capture performance. Finally, to get insight into the role of morphology in CO_2 adsorption, two diverse macroporous structures were synthesized (hydrogels and cryogels) for both HIS and LYS-based materials. As it turns out, hydrogel formulations of an average area ranging from 15.5 to 230 μm^2 adsorb 12% more than cryogels with higher values (266–605 μm^2).

1. Introduction

Climate changes recently experienced by people in several countries, including Europe, are mainly driven by the exponential carbon dioxide (CO_2) emissions in the last eighty years. As well known, this dramatic CO_2 upsurge is derived from the fossil fuel employed for energetic purposes [1]. Human activities have further impacted this process through excessive deforestation of green areas, land clearing for agriculture, and degradation of soils [2]. By waiting to replace fossil fuel with renewable energy sources, a stratagem to be acted consists of sequestering and reutilizing CO_2 in more sustainable processes (e.g., algae growth), partially closing the carbon cycle.

Although still energy-consuming, the main efficient approaches for CO_2 capture are membrane separation [3], cryogenic distillation, and chemical looping [4,5].

The scientific community has been researching advancements in membrane separation since becoming a competitive technology [6]. Nevertheless, poor membrane stability towards acid gases still represents a relevant limit in its utilization. To perform cost-effective technologies for the abatement of CO_2, chemical and physical adsorption has been intensively investigated. Specifically, fluxing the gas streams in an aqueous amine-based solution has proven successful [7]. Indeed, the amines adsorption method can attain CO_2 removal up to 98% [8]. Also, in this case, drawbacks derive from the high energy consumption, corrosion issues, and many adsorber requirements [9]. Therefore, to overcome the stated issues related to amine chemical adsorption, different solid substrates containing them as active groups have been investigated [10–14].

Unlike amines, which chemically interact with CO_2-forming carbamate, the related porous solid materials predominately adsorb CO_2 due

* Corresponding author.
** Corresponding author.
*** Corresponding author.
E-mail addresses: chiara.zagni@unict.it (C. Zagni), sandro.dattilo@cnr.it (S. Dattilo), arescifina@unict.it (A. Rescifina).

https://doi.org/10.1016/j.mtchem.2023.101715
Received 8 June 2023; Received in revised form 28 August 2023; Accepted 3 September 2023
Available online 16 September 2023

to physical interactions [15,16]. Consequently, less energy is required to recharge the sorbent to its initial stage for reuse. In this view, several inorganic (zeolite, silica gel, activated alumina), organic, such as carbon nanotube, microporous polymers, porous organic polymers (POPs), hybrids, and the fascinating metal-organic frameworks (MOFs) were purposely investigated [17].

Although such materials are considered up-to-date for CO_2 [18,19], their large-scale production and applicability are still challenging. Furthermore, their recyclability and eco-sustainability in a vision of less significant harmful materials and processes are unsatisfactory [20].

Recently, gels-based materials have been identified as an emerging class of CO_2 adsorbents owing to their three-dimensional architecture, high surface area, uniform porosity, low mass density, and controllable porous framework [21]. In particular, the pore size and shape can be tuned using different synthetic approaches [22].

Polyethyleneimine (PEI) cryogel containing poly(ethylene glycol) diglycidyl ether (DGE-PEG), 1,4-butanediol diglycidyl ether (DGE-1,4-BD), and glutaraldehyde (GA) as crosslinking agents has been reported as a material with high CO_2 adsorption capacity [23,24]. Liang et al. described the preparation of carbon cryogels from glucose and polyaniline to obtain an excellent CO_2 adsorbent (4.12 mmol g^{-1} at 25 °C and 1 atm). However, its synthesis involves corrosive chemical activating agents [25].

The paper authored by Pruna deals with the formulation of graphene-based cryogels synthesized starting by amine modification of carboxylated graphene oxide via aqueous carbodiimide chemistry. The latter exhibited a CO_2 uptake of 2 mmol/g at 25 °C and 1 atm [26].

Li et al. reported self-activated heteroatom (*N*)-doped carbon cryogels prepared from potassium hydrogen phthalate (KHP) and urea. The obtained material showed remarkable mechanical strength and CO_2 adsorption capacities (280.57 mg/g at 0 °C and 171.31 mg/g at 25 °C at 1 atm) [27].

Although noteworthy, all the works mentioned above involve processes/materials that can compromise an environmentally sustainable production because of a circular economy. In fact, the recyclability of some of the solid adsorbents is often unsatisfactory.

Amine-induced hydrogels (AIHs) are crosslinked materials swelled with aqueous amine solutions (monoethanolamine, MEA, and diethanolamine, DEA) and are useful as carriers for CO_2 absorption under ambient conditions [28]. The advantages of using hydrogels as CO_2 adsorbents are the easiness of preparation, the material's reusability, and a high specific surface area available for reacting and enhancing the absorption kinetics/capacity. Moreover, preparing AIHs is environmentally benign since few wastes and by-products are generated.

Despite the wide availability of the raw materials (MEA, DEA, and hydrogels), the system presents the disadvantage of a limited surface area that could be improved by decreasing the particle size. Amino acid salts (AAS) are considered a promising class of green material for CO_2 capture owing to exceptionally low toxicity, little volatility, and discrete absorption capacity [29,30]. However, their regeneration requires significant energy requirements, limiting their widespread application. To overcome this issue, AAS hydrogel particles were encapsulated into solid polymer matrices to improve their absorption kinetics and storage capacity. So far, hydrogel containing in their structure, chemically linked, the functional group responsible for CO_2 capture has not been reported.

In this paper, we report, as a novelty, the synthesis and application of purposely modified cryogels and hydrogels based on poly-2-hydroxyethyl methacrylate (HEMA) functionalized with aminoacidic moieties. This way, we provide a more sustainable and industrial applicable solution to obtain macroporous polymeric materials for CO_2 capture. Affordable lysine and histidine were used as amine sources to functionalize the well-known polymeric substrate HEMA. In addition, two polymerization procedures were performed and investigated to get insight into the role of gel morphology in CO_2 adsorption. Adsorption ability as a function of the chemical architecture and pore sizes in prepared hydrogels and cryogels were studied and herein discussed.

2. Materials and methods

2.1. Materials

2-Hydroxyethyl methacrylate (HEMA), 2-aminoethyl methacrylate hydrochloride (AEMA), *N*,*N*′-methylene-bis-acrylamide (MBAA), ammonium persulfate (APS), tetramethyl-ethylene-diamine (TEMED), absolute ethanol (EtOH), hydrochloric acid (37%) and sodium hydroxide (NaOH), *N*,*N*′-diisopropylcarbodiimide (DIC), 4-dimethylxamino pyridine (DMAP), trifluoroacetic acid (TFA), dimethylformamide anhydrous (DMF), deuterium oxide (D_2O), and dichloromethane were purchased from Sigma-Aldrich. Boc-Lys(Boc)-OH DCHA and Boc-His (Boc)-OH were obtained from Novabiochem (Hohenbrunn, Germany). A Milli-Q water purification system produced deionized water.

2.2. Synthesis of cryogels and hydrogels

2.2.1. Synthesis of 2-hydroxyethylmethacrylate cryogel (C-HEMA)

500 mg of HEMA (3.8 mmol) was dissolved in water, and crosslinker agent *N*,*N*′-methylene bisacrylamide (MBAA) was added in a molar ratio monomers/crosslinker of 6:1 (99.5 mg, 0.6 mmol) [31]. The mixture was stirred until complete dissolution. The amount of water was then corrected to obtain a total content of polymerizable compounds of 10% w/v of the solution. The mixture was cooled at 0 °C then 1.5% v/v of a water solution of APS at a concentration of 10% w/v was added, followed by the addition of 1.5% v/v of a water solution of TEMED at a concentration of 10% w/v. The mixture was stirred for 1 min, distributed into 10 mL capped syringes, and poured into a cryostatic bath at −15 °C for 24 h. Afterward, the frozen samples were thawed, washed with water and ethanol, and dried under nitrogen flux; then, all samples were dried under vacuum overnight at 40 °C. The polymerization yield was 89% [32].

2.2.2. Synthesis of 2-hydroxyethylmethacrylate hydrogel (H-HEMA)

The synthesis was carried out at room temperature according to the procedure used for the correspondent cryogel synthesis. The previously reported mixture was placed in a vial and, after 24 h, was washed and dried out. The polymerization yield was 92%.

2.2.3. Synthesis of HEMA-LYS cryogel (C-HEMA-LYS)

90 mg (0.186 mmol) of HEMA-LYS, 67.7 μL (0.558 mmol) of HEMA (molar ratio HEMA-LYS/HEMA 3:1), and 19.2 mg (0.124 mmol) of MBAA (molar ratio 1/6 comparing to the moles of monomers) were dissolved in water. NaOH 1.5 N was added to the reaction mixture under vigorous stirring until reaching neutrality. Additional H_2O was added to obtain a total content of polymerizable compounds of 10% w/v of the solution; then, the solution was cooled to 0 °C. Subsequently, 1% v/v (18 μL) of both APS (10% w/v) and TEMED (10% w/v) solutions in water were added under vigorous stirring. The reaction mixture was transferred to a 3 mL capped syringe and placed into a cryostatic bath at −15 °C for 24 h. After 24 h, the cryogel was thawed and washed with mixtures of H_2O/EtOH, progressively increasing the concentration of EtOH up to pure EtOH and finally with Et_2O. The purified cryogel was dried under nitrogen flow and then under vacuum. The final product was obtained with 85% yield and consisted of a macroporous monolithic cryogel.

2.2.4. Synthesis of HEMA-LYS hydrogel (H-HEMA-LYS)

HEMA-LYS hydrogel was prepared with the same procedure as the cryogel but in a vial and at room temperature. The polymerization yield was 87%.

2.2.5. Synthesis of HEMA-HIS cryogel (C-HEMA-HIS)

137 mg (0.2767 mmol) of HEMA-HIS, 102 μL (0.8334 mmol) of HEMA (molar ratio HEMA-HIS/HEMA 3:1), and 28.43 mg (0.1845 mmol) of MBAA (molar ratio 1/6 comparing to the moles of monomers)

were dissolved in water. NaOH 1.5 N was added, reaching neutrality. Additional H_2O was added to obtain a total content of polymerizable compounds of 10% w/v of the solution; then, the solution was cooled to 0 °C. Therefore, 1% v/v (28 μL) of both APS (10% w/v) and TEMED (10% w/v) solutions in water were added under vigorous stirring. Cryopolimerization and drying processes were performed as previously described. The polymerization yield was 84%.

2.2.6. Synthesis of HEMA-HIS hydrogel (H-HEMA-HIS)

The hydrogel was prepared following the same procedure as the cryogel. The mixture was put in a vial, and the reaction proceeded at room temperature. The polymerization yield was 86%.

2.3. Cryogels characterization

All the synthesized materials were accurately characterized. The HEMA-LYS and HEMA-HIS monomer structures were confirmed by ^{1}H and ^{13}C spectra, registered using Varian "Mercury 400" spectrometers, operating at 400 MHz. TMS was used as a reference.

All formulated samples were characterized by Fourier transform infrared spectroscopy (FTIR) spectroscopy. Fourier-transformed spectra were recorded in absorbance mode (64 scans and 4 cm^{-1} resolution) in the 4000–400 cm^{-1} region using a Varian 640-IR by Agilent Technologies, with a ZnSe crystal fixed at the incident angle of 45°.

Morphologies were investigated by scanning electron microscopy (SEM); the samples, previously metalized with a thin layer of gold (<10 nm) to impart their conductivity, were characterized by scanning electric microscopy Thermo Phenom Prox (Thermo Fisher Scientific—Waltham, MA, USA) desktop scanning.

Samples were subjected to thermogravimetric analyses (TGA) by using a thermogravimetric apparatus (TA Instruments Q500) under a nitrogen atmosphere (flow rate 60 mL/min) at 10 °C/min heating rate, from 40 °C to 800 °C. TGA sensitivity is 0.1 μg with a weighting precision of ±0.01%. The isothermal temperature accuracy is ±1 °C.

2.4. CO_2 adsorption and selectivity test

The CO_2 adsorption tests were carried out in a quartz U-shaped reactor filled with 100 mg of the analyzed material flowing CO_2 (99.999%, 30 mL/min) at atmospheric pressure and room temperature. The CO_2 was monitored with a quadrupole mass spectrometer (Sensorlab VG Quadrupoles) following the $m/z = 44$ signal. The adsorption of CO_2 was evaluated by measuring the ratio between the concentration of CO_2 after the saturation in the material and the initial CO_2 concentration. Before the tests, the materials were pretreated in He flows (50 mL/min) at 150 °C for 1 h. With these experimental conditions, the error was within 3%.

The kinetic of CO_2 adsorption was evaluated using a thermogravimetric analyzer (Linseis STA PT 1600 instrument). The materials were degassed under a He stream (50 mL/min) at 150 °C for 1 h. The CO_2 has flowed into the test (30 mL/min), and the weight variation with time was measured.

The CO_2/N_2 adsorption selectivity was measured with the same apparatus, varying the flue gases (15% (v/v) CO_2 and 85% N_2), also following the signals $m/z = 14$ and $m/z = 28$ and maintaining the system at room temperature for 60 min. Following the literature, the selectivity values were determined by the initial kinetic slope ratio (Henry's law constant method) as follows: the first five data points on the single-component adsorption isotherm of CO_2/N_2 were carefully chosen, and the initial slope of each isotherm was evaluated by linear fitting [33]. The adsorption selectivity was calculated as follows:

$$S = k_{CO_2}/k_{N_2}$$

indicating as k_{CO_2} and k_{N_2} the kinetic constants of the CO_2 and the N_2 adsorption, respectively.

2.5. CO_2 desorption

The CO_2 TPD (Temperature Programmed Desorption) measurements were performed with different consecutive runs to determine the reusability of the sample. The tests were carried out in the same reactor previously used. The CO_2 flow was stopped for these measurements after the adsorption and surface saturation processes. Afterward, the reactor was heated from 30 °C to 100 °C (10 °C/min). After desorption, the products were examined with a mass spectrometer. Also, in this case, the samples were pretreated as previously described.

3. Results and discussions

3.1. Synthesis and characterization of hydrogels and cryogels

The poly(HEMA), poly(HEMA-LYS), and poly(HEMA-HIS) cryogels and hydrogels were prepared by the polymerization of the correspondent monomers using MBAA as a crosslinker, according to the chemical reaction given in Fig. 1.

The differences between hydro and cryogels consist in the temperature at which the reaction is carried out. The cryogel formation occurs at a temperature below the freezing point of water. At such a temperature, ice crystals are formed, and the polymerization reaction occurs around the crystals. After the reaction is completed, the system is thawed, melting the crystal and leaving a macroporous structure. Instead, hydrogel's structure, occurring at room temperature, is characterized by a smaller pore dimension. The reaction yield ranges from 84% to 92% in both cases.

The morphological structure of synthesized hydro and cryogels were investigated by SEM analyses. In Fig. 2, SEM micrographs of all synthesized samples are reported. The sample images (Fig. 2a and c–f) reveal the typical structures of these gels consisting of a microporous jagged surface with a random three-dimensional network. Notably, the H-HEMA (Fig. 2b) has a structure constituted by circular nanoaggregate, whose porometric data were reported in Table 1S. As expected, all hydrogels present pore sizes with smaller average dimensions than cryogels (Fig. 3). Among cryogels, C-HEMA-LYS manifests the lowest pores dimensions. Morphological properties influence CO_2 adsorption, as discussed in the next paragraph.

Thermal analysis using TGA was also performed to evaluate the thermal stability of the synthesized cryogels and hydrogels. Table 2 summarizes the results of TGA obtained using N_2 as a carrier gas up to 800 °C. The temperatures at the maximum derivative of weight loss (TMD) range from 420 to 452 °C depending on the monomer's composition.

Thermal profiles of polymer samples revealed a degradation of the main chains in a range of 430–460 °C (Table 1, Figs. S1–S6). Thermal measurements reveal that histidine derivatives manifest higher stability among the materials, most likely due to the heteroaromatic imidazole group within the network [34].

To confirm the success of the polymerizations, FTIR spectra were recorded for all samples (Fig. 4). All the spectra of HEMA and its derivatives (HEMA-LYS and HEMA-HIS) present overlapped peaks in the 3300–3400 cm^{-1} range, corresponding to OH and NH stretching vibrations. A signal at 2955 cm^{-1} is related to CH stretching vibrations, and the peak at 1727 cm^{-1} is assigned to the ester stretching. Finally, the signal at 1652 cm^{-1} was related to the amide crosslinker. The C=O and C–O stretching vibrations in the HEMA-LYS spectrum can be observed at ~1630 cm^{-1} and ~1439 cm^{-1}, respectively [35]. The peak at ~2950 cm^{-1} is due to C–H and N–H stretching vibration overlaps with OH stretching at 3419 cm^{-1}. For HEMA-HIS, the FTIR spectrum indicates similar signals to HEMA-LYS with the amide NH_2 bending vibrations at 1618, 1619, and 729 cm^{-1} [36].

Notably, the disappearance of the typical signal related to methylene (–C=C) groups of the monomers in the range 1000–800 cm^{-1} confirmed the formation of the polymeric cryogel and related hydrogels [37].

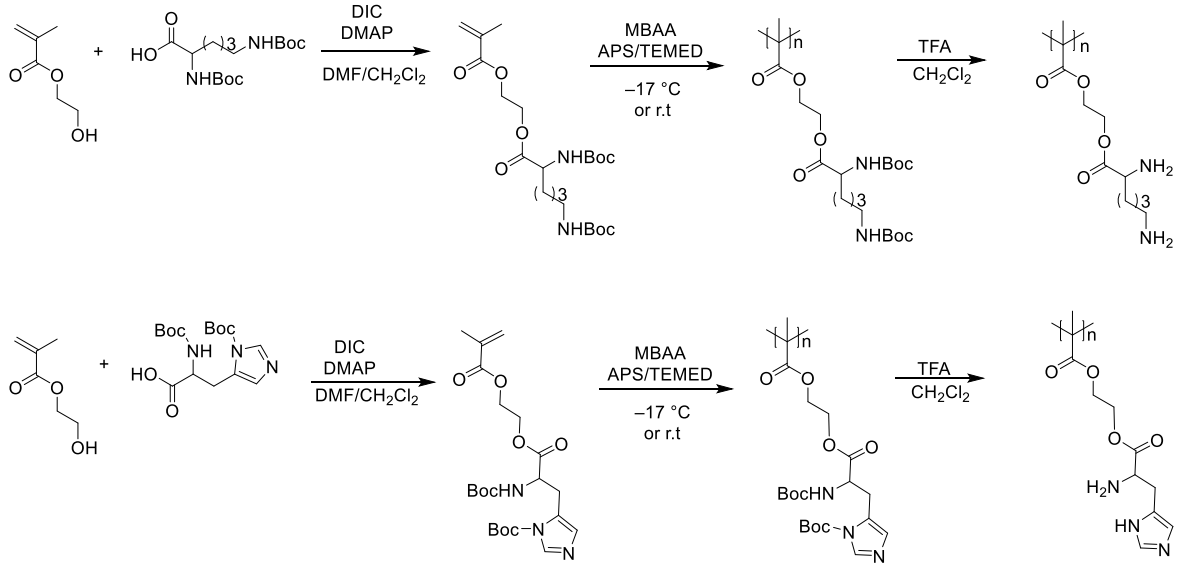

Fig. 1. Schematic representation of HEMA-LYS (top) and HEMA-HIS (bottom) synthesis.

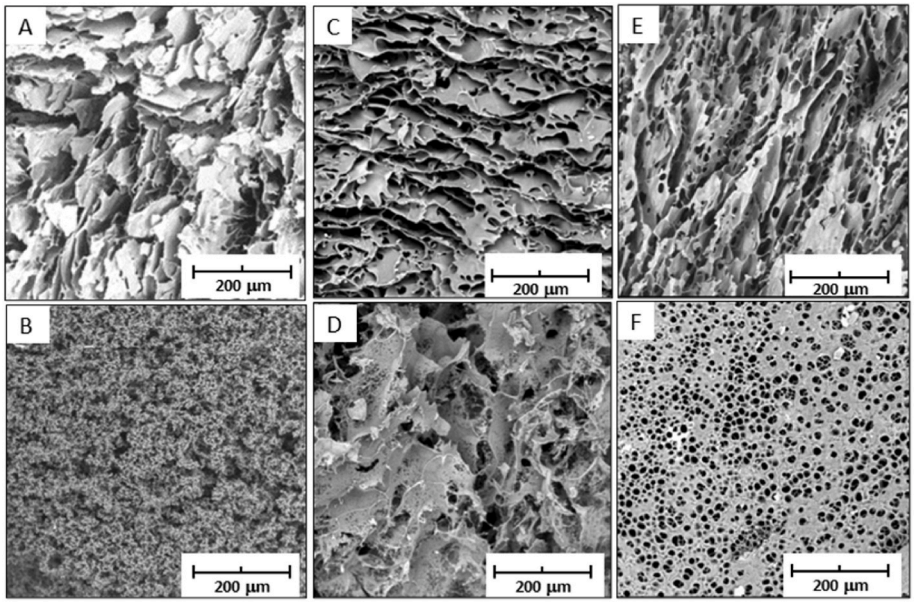

Fig. 2. SEM micrographs of all synthesized samples, a) C-HEMA, b) H-HEMA, c) C-HEMA-LYS, d) H-HEMA-LYS, e) C-HEMA-HIS, f) H-HEMA-HIS.

3.2. CO_2 adsorption and selectivity tests

The adsorption capacities were calculated with Equation (1):

$$q\ (\mathrm{mg/g}) = [(C_{in} - C_f) \times t \times Q]/ \qquad \text{w (1)}$$

where q is the amount of adsorbed CO_2, w is the weight of the analyzed material (g), Q is the CO_2 flow rate (mL/min), t is the saturation time (min), and C_{in} and C_f are the initial and final CO_2 concentrations (mg/mL), respectively [38–40].

As it turns out, the best materials for the CO_2 adsorption are the H-HEMA-LYS (q = 193.0) with similar q values (H-HEMA = 181.0, H-HEMA-HIS = 186.0), whereas the C-HEMA-based samples showed a lower performance.

All prepared materials present high adsorption properties compared to MOR and BEA (Fig. 5) used as reference materials. In addition to the direct comparison with the BEA and MOR, our remarkable results were further highlighted in Table 1, reporting CO_2 capture data of materials stated in recent literature. From the inspection of Fig. 5, material morphology seems to influence the CO_2 adsorption aptitude, achieving better performance for hydrogels. This trend can be ascribable to their lower pore size dimensions obtained by polymerizing with a classical radical reaction. It is reasonable to assume that CO_2 can better physically entrap within the material, while a more suitable reaction time allows its adsorption to the active sites.

Regarding the chemistry of adsorption related to functional groups introduced into as-prepared materials, it is worth noticing that lysine determines higher adsorption capability in both cryogel and hydrogel materials if compared to HEMA and HEMA-HIS. This outcome can derive from the presence of two primary amino groups that increased their electron availability compared to the nitrogen atoms inserted into the imidazole ring in the case of histidine.

The kinetic evaluation of the CO_2 capture was carried out on the H-HEMA-LYS sample as a representative (best) sample (Fig. 6).

As reported, experimental data were fitted with the Linear Driving

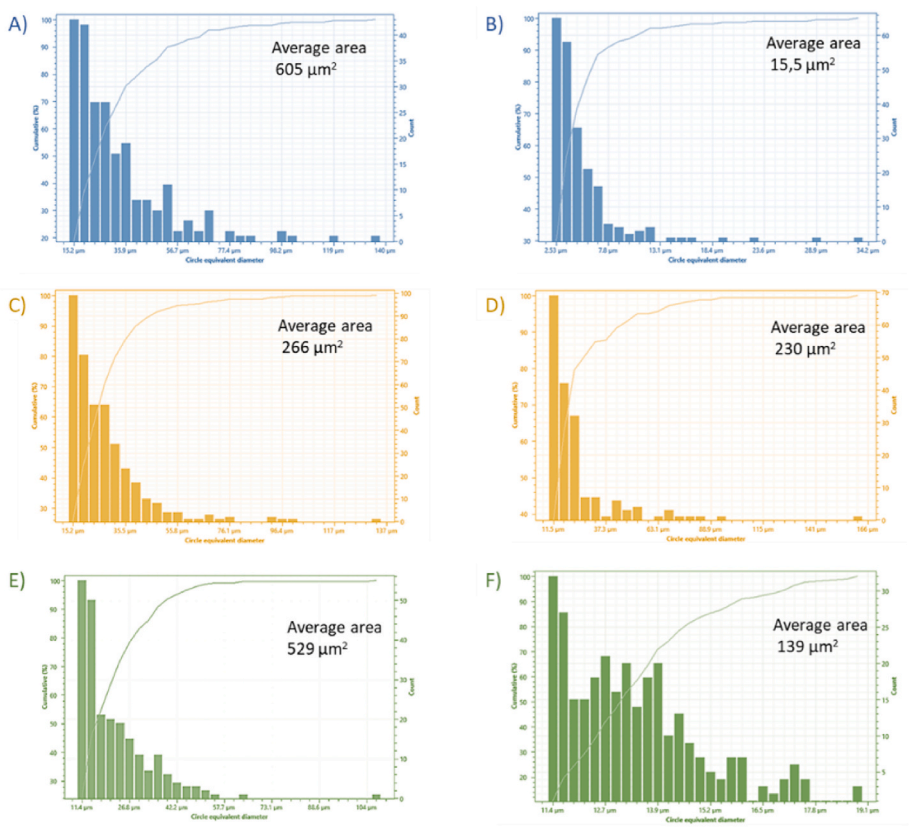

Fig. 3. Cumulative percentage of pore distribution of all samples synthesized A) C-HEMA, B) H-HEMA, C) C-HEMA-LYS, D) H-HEMA-LYS, E) C-HEMA-HIS, F) H-HEMA-HIS calculated using Phenom Porometric 1.1.2.0 (PhenomWorld BV, Eindhoven, The Netherlands).

Table 1
Temperatures at maximum decomposition rate and residual masses of all synthesized samples.

Sample	T_{MD} (°C)	Residue at T = 800 °C (wt%)
C-HEMA	444.3	1.2
C-HEMA-LYS	446.8	1.8
C-HEMA-HIS	451.5	3.2
H-HEMA	445.8	0.6
H-HEMA-LYS	435.6	2.3
H-HEMA-HIS	457.6	2.5

Table 2
Comparison of CO_2 sorption abilities of different materials.

Amide-Based Material	CO_2 Uptake (mg/g)	Reference
C-HEMA	162.0	This work
C-HEMA-LYS	171.5	This work
C-HEMA-HIS	167.5	This work
H-HEMA	181.5	This work
H-HEMA-LYS	193.0	This work
H-HEMA-HIS	186.0	This work
Urease@PEI cryogel	532.4	[41]
Carbon cryogels	198	[42]
Graphene oxide cryogel	88	[43]
PEI-EGDE	501.16	[44]
Porous Carbon	120–180	[45]
BEA	80.5	[46]
CB [6]-Funct	88.4	[46]
PHTCZ-1	59.0	[40]
PHTCZ-2	103.0	[40]
M808-EDTA	64.2	[40]
MOF-1	44.0	[40]
MOF-2	43.6	[40]
MOF-3	82.3	[40]

Force (LDF) and the Pseudo-Second Order (PSO) models [16,38,39].

The LDF model considers the adsorption rate proportional to the number of free surface sites suitable for the adsorption (mainly physisorption). The main driving force of the adsorption process is estimated by the difference between the q at equilibrium and the q at the time t, whereas all the resistances ascribed to the mass transfers are incorporated in the kinetic parameter k_t as global resistance to the diffusion, following the equation in the linear form:

$$\ln (q_e - q_t) = \ln q_e - k_t\, t$$

where q_t and q_e were the amount of CO_2 absorbed per unit mass of the material at time t and at the equilibrium, respectively.

Conversely, in the PSO model, the adsorption is mainly attributed to the chemisorption, following the equation:

$$t/q_t = (1/k_s\, q_e^2 + t/q_e)$$

where k_s is the adsorption rate constant.

From the data reported in Fig. 6, it is possible to note that the LDF model fits better with the experimental data ($R^2 = 0.99$ for the analyzed material), pointing to the reversible physisorption process is mainly involved in the CO_2 adsorption instead of the chemisorption.

To further investigate the ability of the materials to absorb carbon dioxide, infrared spectra have been recorded over the reference compound HEMA-LYS before and after the exposure to CO_2 (Fig. 7). The adsorbtion capacity of the tested samples was confirmed by the presence of a peak at 2424 cm^{-1} that corresponds to the typical asymmetric stretching of the adsorbed CO_2^{-1} [8,39–41]. As a comparison, the spectra of HEMA-LYS, as prepared, were reported (black line), and no signal of CO_2 stretching was revealed.

Table 3 and Fig. 8 report the data for selective adsorption using an N_2/CO_2 mixture obtained by calculating the slope ratio for the H-HEMA-based samples.

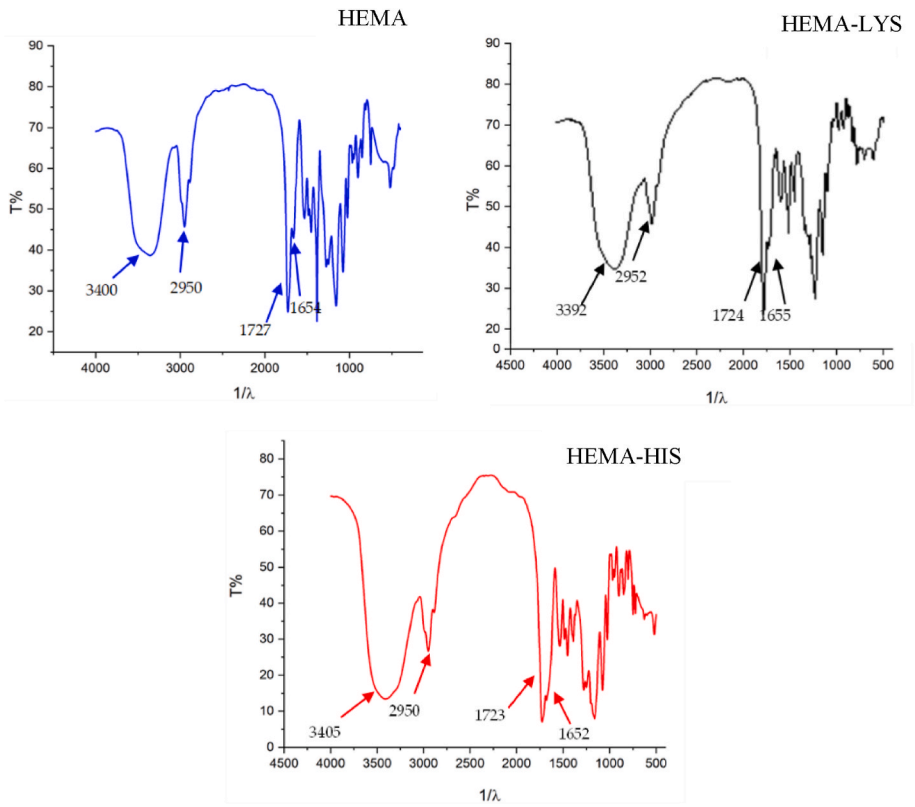

Fig. 4. FT-IR spectra of C-HEMA, C-HEMA-LYS, and C-HEMA-HIS.

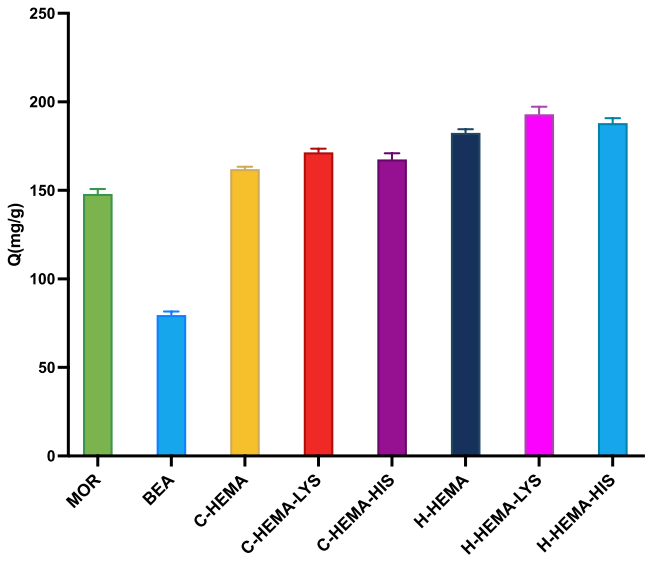

Fig. 5. The CO_2 adsorption capacity of the investigated samples.

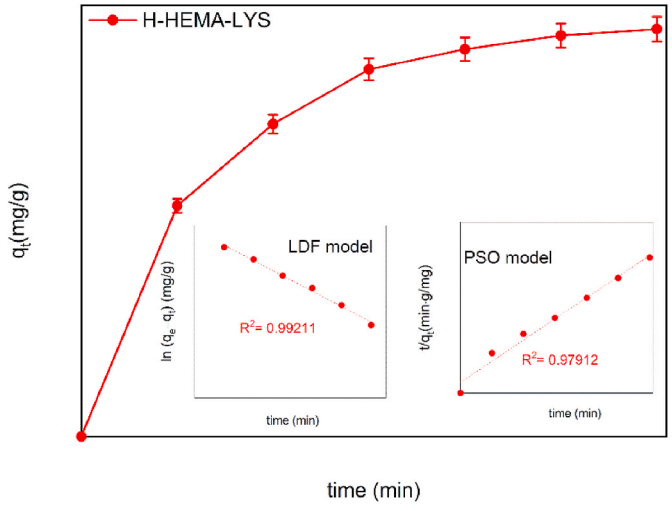

Fig. 6. CO_2 adsorption kinetics on the H-HEMA-LYS sample. The experimental data (points) and the fit (dashed lines) were represented in the insets with the LDF and the PSO models.

It is possible to note that the H-HEMA-LYS sample gave the best selectivity in CO_2 adsorption (S = 20.4); this confirms the synergistic effect of the presence of the lysine group and the suitable pore structure. Furthermore, all the examined samples showed a higher affinity for CO_2 capture than N_2 adsorption.

The reusability features of H-HEMA-LYS were evaluated with five consecutive runs of CO_2 adsorption-desorption measurements. Based on the CO_2-TPD profile of H-HEMA-LYS (Fig. S7, the CO_2 desorption peak was at 37 °C), after the adsorption and the surface saturation of CO_2, the CO_2 flow was stopped, and the sample was heated from room temperature to 100 °C. Therefore, the material was cooled under He flows, and the CO_2 flow was turned on to favor its adsorption to carry out the successive run.

As highlighted in Fig. 9, the CO_2 capture capability of the H-HEMA-LYS was maintained during the five consecutive runs with a decrease of q of only 1.5% compared to the value of the first run. Interestingly, after five consecutive runs, the adsorption ability of the H-HEMA-LYS material was better than that of the standard compounds, such as the BEA and the MOR zeolites (Fig. 5).

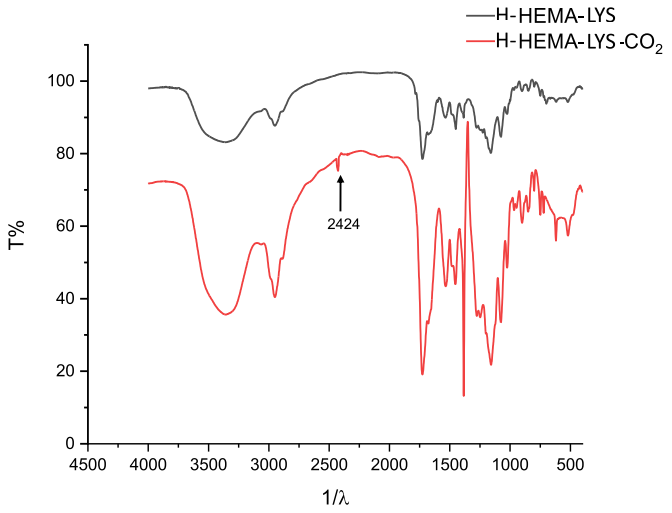

Fig. 7. FT-IR spectra of HEMA-LYS before (black trace) and after (red trace) CO_2 adsorption.

Table 3
Selective adsorption of CO_2 in a N_2/CO_2 mixture for the H-HEMA-based samples.

Sample	kCO_2	kN_2	S (kCO_2/kN_2)
H-HEMA	77.6	4.8	16.1
H-HEMA-LYS	116.5	5.7	20.4
H-HEMA-HIS	86.1	5.1	16.9

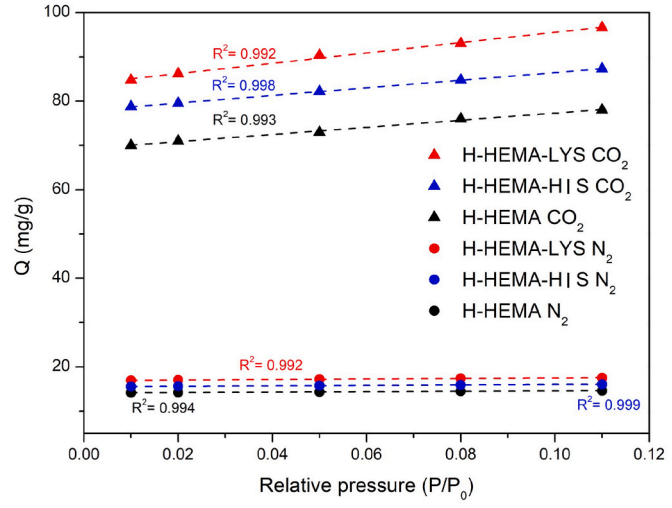

Fig. 8. Initial slope from CO_2 and N_2 adsorption over the examined samples used for the selectivity calculation.

4. Conclusions

Different HEMA-based hydrogels and cryogels functionalized with basic amino acids (LYS and HIS) have been successfully synthesized by chain polymerization using water as a solvent. The synthesized materials were characterized by IR, TG, SEM, and EDX, assessing the formation of desired acrylic polymers. Adsorption test performed at 25 °C demonstrated a significant aptitude of all materials in sequestering CO_2.

Remarkably, H-HEMA-LYS provides a value of CO_2 adsorption of 193 mg/g, sensibly higher by 32% and 140% compared to MOR and BEA, respectively, used as reference materials and recent findings reported in the literature (Fig. 5).

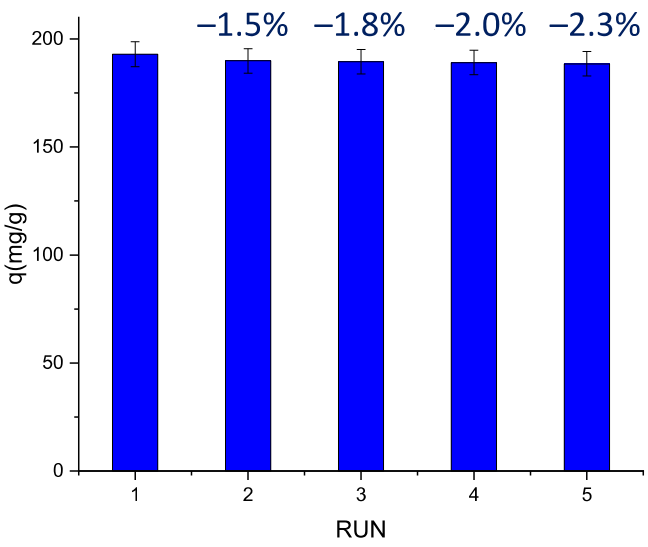

Fig. 9. Reusability features of H-HEMA-LYS up to five runs.

Data obtained also suggest that pores sizes influence the adsorption phenomena. Specifically, lower pore size allows better results in capturing CO_2 if compared to cryogel pores.

Further, ulteriorly modifying HEMA-based polymers might improve the adsorption parameters and CO_2 adsorption capacity through appropriate activation.

CRediT authorship contribution statement

Chiara Zagni: Conceptualization, Investigation, Methodology, Visualization, Writing – original draft, Writing – review & editing. **Alessandro Coco:** Investigation, Validation. **Sandro Dattilo:** Data curation, Visualization, Writing – review & editing. **Vincenzo Patamia:** Investigation. **Giuseppe Floresta:** Visualization, Writing – review & editing. **Roberto Fiorenza:** Formal analysis, Investigation, Visualization, Funding acquisition, Writing - original draft. **Giusy Curcuruto:** Data curation, Writing – review & editing. **Tommaso Mecca:** Conceptualization, Visualization. **Antonio Rescifina:** Supervision, Project administration, Funding acquisition, Writing – review & editing.

Declaration of competing interest

The authors declare that they have no known competing financial interests or personal relationships that could have appeared to influence the work reported in this paper.

Data availability

No data was used for the research described in the article.

Acknowledgements

The research leading to these results has received funding from the EU-funded PON REACT project Azione IV.6 – "Contratti di ricerca su tematiche green" del nuovo Asse IV del PON Ricerca e Innovazione 2014–2020 "Istruzione e ricerca per il recupero – REACT – EU"; Progetto "CO_2 as C_1 renewable source for innovative sustainable synthetic approaches: from small molecules to materials", (Antonio Rescifina and Chiara Zagni), CUP: E61821004320005.

Roberto Fiorenza thanks PIA.CE.RI. 2020–2022 Linea 3 DOBLE-CO2RE Starting Grant project of the University of Catania for the support.

Appendix A. Supplementary data

Supplementary data to this article can be found online at https://doi.org/10.1016/j.mtchem.2023.101715.

References

[1] R. Nataly Echevarria Huaman, T. Xiu Jun, Energy related CO2 emissions and the progress on CCS projects: a review, Renew. Sustain. Energy Rev. 31 (2014) 368–385, https://doi.org/10.1016/j.rser.2013.12.002.

[2] B.L. Salvi, S. Jindal, Recent developments and challenges ahead in carbon capture and sequestration technologies, SN Appl. Sci. 1 (2019) 885, https://doi.org/10.1007/s42452-019-0909-2.

[3] G. Chen, T. Wang, G. Zhang, G. Liu, W. Jin, Membrane materials targeting carbon capture and utilization, Adv. Membr. 2 (2022), 100025, https://doi.org/10.1016/j.advmem.2022.100025.

[4] X. He, A review of material development in the field of carbon capture and the application of membrane-based processes in power plants and energy-intensive industries, Energy Sustain. Soc. 8 (2018) 34, https://doi.org/10.1186/s13705-018-0177-9.

[5] V. Patamia, R. Tomarchio, R. Fiorenza, C. Zagni, S. Scirè, G. Floresta, A. Rescifina, Carbamoyl-decorated cyclodextrins for carbon dioxide adsorption, Catalysts 13 (2023) 41, https://doi.org/10.3390/catal13010041.

[6] R. Bredesen, K. Jordal, O. Bolland, High-temperature membranes in power generation with CO2 capture, Chem. Eng. Process: Process Intensif. 43 (2004) 1129–1158, https://doi.org/10.1016/j.cep.2003.11.011.

[7] N. Harun, T. Nittaya, P.L. Douglas, E. Croiset, L.A. Ricardez-Sandoval, Dynamic simulation of MEA absorption process for CO2 capture from power plants, Int. J. Greenh. Gas Control 10 (2012) 295–309, https://doi.org/10.1016/j.ijggc.2012.06.017.

[8] J.T. Yeh, K.P. Resnik, K. Rygle, H.W. Pennline, Semi-batch absorption and regeneration studies for CO2 capture by aqueous ammonia, Fuel Process. Technol. 86 (2005) 1533–1546, https://doi.org/10.1016/j.fuproc.2005.01.015.

[9] A.A. Abd, S.Z. Naji, Comparison study of activators performance for MDEA solution of acid gases capturing from natural gas: simulation-based on a real plant, Environ. Technol. Innov. 17 (2020), 100562, https://doi.org/10.1016/j.eti.2019.100562.

[10] M. Keramati, A.A. Ghoreyshi, Improving CO2 adsorption onto activated carbon through functionalization by chitosan and triethylenetetramine, Phys. E Low-dimens. Syst. Nanostruct. 57 (2014) 161–168, https://doi.org/10.1016/j.physe.2013.10.024.

[11] X. Xu, C. Song, J.M. Andresen, B.G. Miller, A.W. Scaroni, Novel polyethylenimine-modified mesoporous molecular sieve of MCM-41 type as high-capacity adsorbent for CO2 capture, Energy Fuels 16 (2002) 1463–1469, https://doi.org/10.1021/ef020058u.

[12] X. Xu, C. Song, J.M. Andrésen, B.G. Miller, A.W. Scaroni, Preparation and characterization of novel CO2 "molecular basket" adsorbents based on polymer-modified mesoporous molecular sieve MCM-41, Microporous Mesoporous Mater. 62 (2003) 29–45, https://doi.org/10.1016/S1387-1811(03)00388-3.

[13] A. Ahmadalinezhad, A. Sayari, Oxidative degradation of silica-supported polyethylenimine for CO2 adsorption: insights into the nature of deactivated species, Phys. Chem. Chem. Phys. 16 (2013) 1529–1535, https://doi.org/10.1039/C3CP53928H.

[14] G. Qi, Y. Wang, L. Estevez, X. Duan, N. Anako, A.-H.A. Park, W. Li, C.W. Jones, E. P. Giannelis, High efficiency nanocomposite sorbents for CO2 capture based on amine-functionalized mesoporous capsules, Energy Environ. Sci. 4 (2011) 444–452, https://doi.org/10.1039/C0EE00213E.

[15] S.-Y. Lee, S.-J. Park, A review on solid adsorbents for carbon dioxide capture, J. Ind. Eng. Chem. 23 (2015) 1–11, https://doi.org/10.1016/j.jiec.2014.09.001.

[16] V. Patamia, R. Fiorenza, I. Brullo, M. Zambito Marsala, S.A. Balsamo, A. Distefano, P.M. Furneri, V. Barbera, S. Scirè, A. Rescifina, A sustainable porous composite material based on loofah-halloysite for gas adsorption and drug delivery, Mater. Chem. Front. 6 (2022) 2233–2243, https://doi.org/10.1039/d2qm00505k.

[17] X. Zou, G. Zhu, Microporous organic materials for membrane-based gas separation, Adv. Mater. 30 (2018), 1700750, https://doi.org/10.1002/adma.201700750.

[18] K.S. Song, P.W. Fritz, A. Coskun, Porous organic polymers for CO2 capture, separation and conversion, Chem. Soc. Rev. 51 (2022) 9831–9852, https://doi.org/10.1039/D2CS00727D.

[19] L. Li, H.S. Jung, J.W. Lee, Y.T. Kang, Review on applications of metal–organic frameworks for CO2 capture and the performance enhancement mechanisms, Renew. Sustain. Energy Rev. 162 (2022), 112441, https://doi.org/10.1016/j.rser.2022.112441.

[20] X. Xu, C. Heath, B. Pejcic, C.D. Wood, CO2 capture by amine infused hydrogels (AIHs), J. Mater. Chem. A 6 (2018) 4829–4838, https://doi.org/10.1039/C8TA00602D.

[21] G. Nazir, A. Rehman, S.-J. Park, Self-activated, urea modified microporous carbon cryogels for high-performance CO2 capture and separation, Carbon 192 (2022) 14–29, https://doi.org/10.1016/j.carbon.2022.02.040.

[22] O. Okay (Ed.), Polymeric Cryogels, Springer International Publishing, Cham, 2014, https://doi.org/10.1007/978-3-319-05846-7.

[23] C.-J. Yoo, P. Narayanan, C.W. Jones, Self-supported branched poly(ethyleneimine) materials for CO2 adsorption from simulated flue gas, J. Mater. Chem. A 7 (2019) 19513–19521, https://doi.org/10.1039/C9TA04662C.

[24] Y. Chen, X. Qiu, H. Liu, S. Chen, Preparation of a laminated structured polyethyleneimine cryogel for carbon capture, J. Environ. Manag. 317 (2022), 115400, https://doi.org/10.1016/j.jenvman.2022.115400.

[25] L. Liang, M. Zhou, K. Li, L. Jiang, Facile and fast polyaniline-directed synthesis of monolithic carbon cryogels from glucose, Microporous Mesoporous Mater. 265 (2018) 26–34, https://doi.org/10.1016/j.micromeso.2018.01.035.

[26] A.I. Pruna, A. Barjola, A.C. Cárcel, B. Alonso, E. Giménez, Effect of varying amine functionalities on CO2 capture of carboxylated graphene oxide-based cryogels, Nanomaterials 10 (2020) 1446, https://doi.org/10.3390/nano10081446.

[27] Z. Li, T. Chen, X. Wu, L. Luo, Z. Zhang, Z. Li, M. Fan, Z. Su, W. Zhao, Nitrogen-containing high surface area carbon cryogel from co-condensed phenol–urea–formaldehyde resin for CO2 capture, J. Porous Mater. 26 (2019) 847–854, https://doi.org/10.1007/s10934-018-0680-6.

[28] X. Xu, C. Heath, B. Pejcic, C.D. Wood, CO2 capture by amine infused hydrogels (AIHs), J. Mater. Chem. A 6 (2018) 4829–4838, https://doi.org/10.1039/C8TA00602D.

[29] X. Xu, M.B. Myers, F.G. Versteeg, E. Adam, C. White, E. Crooke, C.D. Wood, Next generation amino acid technology for CO2 capture, J. Mater. Chem. A 9 (2021) 1692–1704, https://doi.org/10.1039/D0TA10583J.

[30] E. Scamporrino, P. Mineo, S. Dattilo, D. Vitalini, E. Spina, Uncharged water-soluble metal-bis-porphyrins like molecular tweezers for amino acids, Macromol. Rapid Commun. 28 (2007) 1546–1552, https://doi.org/10.1002/marc.200700234.

[31] C. Zagni, A.A. Scamporrino, P.M. Riccobene, G. Floresta, V. Patamia, A. Rescifina, S.C. Carroccio, Portable nanocomposite system for wound healing in space, Nanomaterials 13 (2023) 741, https://doi.org/10.3390/nano13040741.

[32] C. Zagni, A. Coco, T. Mecca, G. Curcuruto, V. Patamia, K. Mangano, A. Rescifina, S. C. Carroccio, Sponge-like macroporous cyclodextrin-based cryogels for controlled drug delivery, Mater. Chem. Front. (2023), https://doi.org/10.1039/D3QM00139C.

[33] Y. Zhou, L. Luo, W. Yan, Z. Li, M. Fan, G. Du, W. Zhao, Controlled preparation of nitrogen-doped hierarchical carbon cryogels derived from Phenolic-Based resin and their CO2 adsorption properties, Energy 246 (2022), 123367, https://doi.org/10.1016/j.energy.2022.123367.

[34] M. Ussia, A. Di Mauro, T. Mecca, F. Cunsolo, G. Nicotra, C. Spinella, P. Cerruti, G. Impellizzeri, V. Privitera, S.C. Carroccio, ZnO-pHEMA nanocomposites: an ecofriendly and reusable material for water remediation, ACS Appl. Mater. Interfaces 10 (2018) 40100–40110, https://doi.org/10.1021/acsami.8b13029.

[35] A. Ebrahiminezhad, G. Younes, S. Rasoul-Amini, J. Barar, S. Davaran, Impact of amino-acid coating on the synthesis and characteristics of iron-oxide nanoparticles (IONs), Bull. Kor. Chem. Soc. 33 (2012), https://doi.org/10.5012/bkcs.2012.33.12.3957.

[36] A. Ghosh, M.J. Tucker, F. Gai, 2D IR spectroscopy of histidine: probing side-chain structure and dynamics via backbone amide vibrations, J. Phys. Chem. B 118 (2014) 7799–7805, https://doi.org/10.1021/jp411901m.

[37] C. Zagni, S. Dattilo, T. Mecca, C. Gugliuzzo, A.A. Scamporrino, V. Privitera, R. Puglisi, S. Carola Carroccio, Single and dual polymeric sponges for emerging pollutants removal, Eur. Polym. J. 179 (2022), https://doi.org/10.1016/j.eurpolymj.2022.111556.

[38] L. Stevens, K. Williams, W.Y. Han, T. Drage, C. Snape, J. Wood, J. Wang, Preparation and CO2 adsorption of diamine modified montmorillonite via exfoliation grafting route, Chem. Eng. J. 215–216 (2013) 699–708, https://doi.org/10.1016/j.cej.2012.11.058.

[39] E. Gomez-Delgado, G.V. Nunell, A.L. Cukierman, P.R. Bonelli, Influence of the carbonization atmosphere on the development of highly microporous adsorbents tailored to CO2 capture, J. Energy Inst. 102 (2022) 184–189, https://doi.org/10.1016/j.joei.2022.03.003.

[40] C. Lu, H. Bai, B. Wu, F. Su, J.F. Hwang, Comparative study of CO $_2$ capture by carbon nanotubes, activated carbons, and zeolites, Energy Fuels 22 (2008) 3050–3056, https://doi.org/10.1021/ef8000086.

[41] S. Demirci, N. Sahiner, Urease-immobilized PEI cryogels for the enzymatic hydrolysis of urea and carbon dioxide uptake, Ind. Eng. Chem. Res. 61 (2022), https://doi.org/10.1021/acs.iecr.1c05087.

[42] Z. Li, Y. Zhou, W. Yan, L. Luo, Z. Su, M. Fan, S. Wang, W. Zhao, Cost-effective monolithic hierarchical carbon cryogels with nitrogen doping and high-performance mechanical properties for CO2 capture, ACS Appl. Mater. Interfaces 12 (2020) 21748–21760, https://doi.org/10.1021/acsami.0c04015.

[43] A.I. Pruna, A. Barjola, A.C. Cárcel, B. Alonso, E. Giménez, Effect of varying amine functionalities on CO2 capture of carboxylated graphene oxide-based cryogels, Nanomaterials 10 (2020) 1446, https://doi.org/10.3390/nano10081446.

[44] Y. Chen, X. Qiu, H. Liu, S. Chen, Preparation of a laminated structured polyethyleneimine cryogel for carbon capture, J. Environ. Manag. 317 (2022), 115400, https://doi.org/10.1016/j.jenvman.2022.115400.

[45] G. Nazir, A. Rehman, S.-J. Park, Self-activated, urea modified microporous carbon cryogels for high-performance CO2 capture and separation, Carbon 192 (2022) 14–29, https://doi.org/10.1016/j.carbon.2022.02.040.

[46] V. Patamia, D. Gentile, R. Fiorenza, V. Muccilli, P.G. Mineo, S. Scirè, A. Rescifina, Nanosponges based on self-assembled starfish-shaped cucurbit[6]urils functionalized with imidazolium arms, Chem. Commun. 57 (2021) 3664–3667, https://doi.org/10.1039/d1cc00990g.